

Numerical simulation of solid particle ablation in thermal plasmas using CIP-VOF Method

著者	Tanaka Yasunori, Mostaghimi Javad T.
journal or publication title	IEEJ Transactions on Electrical and Electronic Engineering
volume	4
number	4
page range	488-496
year	2009-07-01
URL	http://hdl.handle.net/2297/23877

doi: 10.1002/tee.20434

Numerical Simulation of Solid Particle Ablation in Thermal Plasmas using CIP-VOF Method

Yasunori Tanaka* Member
Javad Mostaghimi** Non-member

Numerical modelling was performed for ablation processing of a solid particle in a thermal plasma flow. The model is based on Constrained Interpolation Propagation – Combined and Unified Procedure (CIP-CUP) method, which can simulate incompressible and compressible flows and then the multiphase flow. Furthermore, the volume of fraction (VOF) function was introduced to track the surface of the solid during ablation. Using that developed model, the ablation process of a polyethylene particle was simulated in a thermal plasma flow. Results show that ablation occurs more strongly at the particle's upstream surface, thereby producing strong gas flow.

Keywords: CIP, VOF, Ablation, Thermal plasma, Particles, Interactions

1. Introduction

In recent years, thermal plasmas have become widely used for various material-processing technologies such as nanopowder synthesis, thermal plasma spray coating, and powder spheroidization. In these processes, raw materials are injected as powders into the plasma. They are subsequently accelerated, heated, melted, and evaporated. Evaporation/sublimation affects the interaction between solid materials and surrounding thermal plasmas because it absorbs thermal energy from the plasma and might then decrease the temperature of the solid surface. It can also modify the gas flow and density fields around the surface of the particles because of ablation phenomena, which might shield the particle surface from heat transfer from the plasma. The phenomena described above are closely related with the heating efficiency of the powder by the plasma. Moreover, the particle surface shape can change by its sublimation/evaporation, which might also alter the efficiency described above.

Such interactions between thermal plasma and solid matter are readily apparent in various thermal plasma or arc plasma application fields. Arc plasma invariably necessitates the use of electrodes, and interactions exist between the arc plasma and the electrode materials. Another example is an ablator, which is designed to protect the reentry capsule from high temperatures by aerodynamic heating between the capsule and the atmospheric air when a reentry capsule returns from space to the earth⁽¹⁾.

To understand the above-described interactions be-

tween thermal plasma and a solid material, it is important to model physical phenomena in detail including the phase transition between solid, gas, and plasmas self-consistently, incorporating gas flow and temperature field solutions. However, these phenomena are very complicated. For that reason, the interactions between thermal plasma and solid materials have remained unclear. Especially, experimental techniques cannot be used for elucidation of these complex phenomena: numerical simulation is necessary for this purpose.

In this work, we present development of our computational model, which is useful to study the ablation of a particle immersed in a thermal plasma based on the Constrained Interpolation Propagation – Combined and Unified Procedure (CIP-CUP) method developed by Yabe⁽²⁾⁽³⁾. The CIP-CUP method is a unified algorithm that is useful to solve incompressible and compressible flow. For that reason, it can simulate multiphase flows including solid, liquid, and gas components. Rapid ablation can eject much ablated vapor with a high gas flow velocity, which might be treated as a compressible flow, although the surrounding gas is almost an incompressible flow. Furthermore, the volume of fluid (VOF) function⁽⁴⁾ was adopted to track the boundary between solid and gas in this work. This is the first paper to describe modeling of solid ablation phenomena in thermal plasmas. Consequently, the methodology to treat gas flow is described first in this paper, with subsequent explanations of the ablation phenomenon and the shape change of the solid boundary.

Using the developed model, the ablation process of a polyethylene spherical particle in an Ar thermal plasma was simulated. This issue is treated here because polymer materials have a lower thermal decomposition temperature and a lower latent heat than other materials, such as metals, do. These lower values permit it to be ablated rapidly by heat flux. This rapid ablation mate-

* Division of Electrical Engineering & Computer Science, Kanazawa University, Kakuma, Kanazawa 920-1192, Japan

** Centre for Advanced Coating Technologies, University of Toronto, 40 St. George Street, Toronto, Ontario, Canada, M5S 3G8 Canada

rial is suitable for fundamental studies of ablation phenomena. Moreover, to date, we have studied ablation phenomena of solid polymer particle in thermal plasmas experimentally to investigate effects of ablated vapor on quenching of thermal plasmas⁽⁵⁾, and in which the interactions between polymer powders and the thermal plasmas are important for the fundamental study of ablated vapor effects on the plasma temperature in our previous paper⁽⁵⁾. The calculation results presented herein demonstrate that strong ablation occurs at the upstream particle surface, which produces a strong gas flow; then the particle shape changes with time.

2. Modeling

2.1 Assumption This expository work addresses the thermal sublimation/evaporation of a solid particle in the thermal plasma flow. This system is expected to include solid, liquid, gas, and thermal plasma. However, the following assumptions were made for simplicity: (i) The thermal plasma around the solid particle is assumed to be under local thermodynamic equilibrium conditions. In this case, the temperatures of the electron and the heavy particle, the excitation temperature, etc. are identical. Furthermore, it is assumed that all the reactions reach their equilibrium condition instantly. (ii) The plasma is assumed to be optically thin. (iii) The plasma and gas are treated as a continuum because of the low Knudsen number Kn . In this work, $Kn \sim 1/30$. (iv) One fluid model is adopted for the plasma, which means that the electrons and the heavy particles including ions, neutral atoms and molecules move with equal gas flow velocity. (v) Melting phenomena of the particles are neglected. Only sublimation is considered. (vi) Ablation of the solid surface is caused only by heat, not directly by radiation from the plasmas. (vii) Charging effects of the particle and the electron emission process from the solid particle are neglected. (viii) Cracking and breaking phenomena of the solid particle are neglected. (ix) Physical and chemical sputtering are neglected.

2.2 Governing equations Herein we deal with the solid, gas, and thermal plasma using the following set of fluid equations.

Mass conservation:

$$\frac{D\rho}{Dt} = -\rho(\nabla \cdot \mathbf{u}) \dots\dots\dots (1)$$

Momentum conservation:

$$\rho \frac{D\mathbf{u}}{Dt} = -\nabla p + \nabla : \tau \dots\dots\dots (2)$$

Energy conservation:

$$\rho C_v \frac{DT}{Dt} = -p_{th}(\nabla \cdot \mathbf{u}) + Q_{heat} - S_{sub} \dots\dots\dots (3)$$

Mass fraction of ablated vapor from the solid:

$$\rho_g \frac{DY_C}{Dt} = \nabla \cdot (\rho_g D_j \nabla Y_C) + S_{C_g} \dots\dots\dots (4)$$

Volume fraction:

$$\frac{Df}{Dt} = -S_f \dots\dots\dots (5)$$

In addition, we use the equation of state (EOS) $p = p(\rho, T)$ for Ar gas and ablated vapor from the solid particle, and that of the solid. Therein, the variables represent the following. $D/Dt = \partial/\partial t + \mathbf{u} \cdot \nabla$: the substantial derivative, t : time, ρ : total mass density in a control volume, ρ_g : mass density of gas in a control volume, \mathbf{u} : the flow velocity vector, p : pressure, τ : stress tensor, T : temperature, Q_{heat} : heating power, D_C : effective diffusion coefficient of ablated vapor against Ar, C_v : specific heat at constant volume, Y_C : mass fraction of ablated vapor in reference to the total gas (Ar gas + ablated vapor) in a control volume, S_{C_g} : source term for ablated vapor mass fraction Y_C by sublimation, f : VOF function, S_f : source term for the VOF function f by sublimation, S_{sub} : sublimation loss. Quantity p_{th} is defined as

$$p_{th} = T \left(\frac{\partial p}{\partial T} \right)_\rho \dots\dots\dots (6)$$

The VOF function f is assumed to be unity when a cell is fully occupied by the solid, and zero when a cell is fully occupied by the gas. Cells with values of $0 < f < 1$ contain a solid surface.

2.3 Source terms

2.3.1 Heating power Heating power Q_{heat} in Eq. (3) was calculated considering thermal conduction and radiation loss as

$$Q_{heat} = \begin{cases} \nabla \cdot (\lambda \nabla T) - P_{rad} \\ -\varepsilon_{emit} \sigma_{sb} (T^4 - T_a^4) \frac{\Delta S}{\Delta V} & (\text{if } \ell > \epsilon_1) \\ \nabla \cdot (\lambda \nabla T) - P_{rad} & (\text{otherwise}) \end{cases}$$

where λ : thermal conductivity, P_{rad} : volume radiation loss, σ_{sb} : Stefan-Boltzmann's constant, T_a : ambient temperature, ε_{emit} : emissivity of the solid surface, ϵ_1 : the positive value to track the solid surface, ΔS : surface area of the solid in a control volume, ΔV : volume of a control volume.

The quantity ℓ is introduced as a parameter used to detect the surface of the solid particle, which is expressed as

$$\ell = \sum_{\alpha, \beta} |f_{\alpha, \beta} - f_{i, j}|, \dots\dots\dots (7)$$

where $\alpha = i - 1, i + 1$ and $\beta = j - 1, j + 1$. Point (i, j) is recognized as the solid surface if ℓ has a non-zero value.

2.3.2 Source term S_f for f The source term by sublimation and deposition on the solid surface in Eq. (5) was incorporated as follows.

$$S_f = S_f^{sub} + S_f^{dep} \dots\dots\dots (8)$$

$$S_f^{sub} = \begin{cases} \max(0, \frac{Q_{heat}}{\rho_s^{mat} L}) & (\text{if } f > \epsilon_2 \text{ \& } T \geq T_{sub} \text{ \& } \ell > \epsilon_3) \\ 0 & (\text{otherwise}) \end{cases} \dots\dots (9)$$

$$S_f^{dep} = \begin{cases} \min(0, \frac{Q_{heat}}{\rho_s^{mat} L}) & (\rho_g Y_C R_C T \geq P_{sat} \text{ \& } \ell > \epsilon_3) \\ 0 & (\text{otherwise}) \end{cases} \dots\dots (10)$$

Therein, S_f^{sub} and S_f^{dep} respectively signify the source terms for sublimation and deposition, and L represents the latent heat for sublimation, ρ_s^{mat} is the mass density of the solid as a material, T_{sub} is the sublimation temperature, R_C is the gas constant of the ablated vapor, P_{sat} is the saturation vapor pressure of the solid material, ϵ_2 and ϵ_3 are small positive values used to track the solid surface. A constraint for $S_f \Delta t$ is that

$$-\frac{\rho_g}{\rho_s^{\text{mat}}} < S_f \Delta t < f, \dots \dots \dots (11)$$

where Δt is the time step for calculation.

2.3.3 Source term S_{C_g} for Y_C The quantity S_{C_g} was calculated using S_f as

$$S_{C_g} = \frac{\rho_g}{\Delta t} (1 - Y_C) \frac{S_f \Delta t \rho_s^{\text{mat}}}{\rho_g + S_f \Delta t \rho_s^{\text{mat}}} \dots \dots \dots (12)$$

2.3.4 Energy loss by sublimation S_{sub} Sublimation requires energy S_{sub} that has been added in the energy conservation equation (3). This term S_{sub} is estimated as

$$S_{\text{sub}} = S_f L \rho_s^{\text{mat}} \dots \dots \dots (13)$$

3. Solution procedure

To solve the equations introduced in the previous section, the time-splitting method was adopted. Time-splitting was done in three phases: advection, diffusion, and isentropic.

The advection phase corresponds to advection phenomena of all physical parameters by gas flow. The non-advection phase gives thermodynamic change in matter. This non-advection phase was separated further into two parts—the diffusion phase and isentropic phase—as described below. It is important to consider a generalized thermodynamic parameter Θ . This parameter can be a function of two other thermodynamic parameters like mass density ρ and entropy S . It therefore brings $\Theta = \Theta(\rho, S)$. If one considers the exact differential $d\Theta$, it can be written as

$$d\Theta = \left(\frac{\partial \Theta}{\partial \rho} \right)_S d\rho + \left(\frac{\partial \Theta}{\partial S} \right)_\rho dS \dots \dots \dots (14)$$

This expression shows that $d\Theta$ contains a change in Θ by S with ρ fixed, and that by ρ with S fixed. These phenomena correspond respectively to the diffusion phase with an entropy change and the isentropic phase.

(i) Advection phase

In this phase, all physical parameters are only advected with the flow velocity \mathbf{u} according to the following advection equation.

$$\frac{D\mathbf{F}}{Dt} = \frac{\partial \mathbf{F}}{\partial t} + \mathbf{u} \cdot \nabla \mathbf{F} = 0 \dots \dots \dots (15)$$

Therein, $\mathbf{F} = (\rho, \mathbf{u}, T, Y_C, f)$. Those components correspond respectively to the mass, momentum, energy equations, and the mass equations for ablated vapor, and the equation of the VOF function. This advection equation was solved using the CIP and rational CIP (R-CIP) algorithms developed by Yabe⁽²⁾⁽³⁾ The pressure

was also advected using the EOS $p = p(\rho, T)$. The CIP algorithm is well known to realize a slightly diffusive scheme for advection.

(ii) Diffusion phase

In this diffusion phase, diffusive processes were considered, including the viscous force for the momentum equation, the thermal conduction, the input power and loss for the energy equation, and the phase transition phenomena, where the total mass density ρ in a control volume is fixed as follows.

Mass equation:

$$\frac{\partial \rho}{\partial t} = 0 \dots \dots \dots (16)$$

Momentum equation:

$$\rho \frac{\partial \mathbf{u}}{\partial t} = \nabla : \boldsymbol{\tau} \dots \dots \dots (17)$$

Energy equation:

$$\rho C_v \frac{\partial T}{\partial t} = Q_{\text{heat}} - S_{\text{sub}} \dots \dots \dots (18)$$

Mass fraction of ablated vapor:

$$\rho_g \frac{\partial Y_C}{\partial t} = \nabla \cdot (\rho_g D_C \nabla Y_C) + S_{C_g} \dots \dots \dots (19)$$

VOF function:

$$\frac{\partial f}{\partial t} = -S_f \dots \dots \dots (20)$$

The equations shown above for the diffusion phase were solved with the full implicit method using values after the advection phase. The pressure rise Δp occurs by the temperature rise and the phase transition, whereas the total mass density ρ in a control volume is constant in this diffusion phase according to Eq. (16). The pressure increase Δp in a control volume was estimated through EOS as

$$\Delta p = \Delta \rho_g R_C T + p_{\text{th}} \frac{\Delta T}{T} \dots \dots \dots (21)$$

$$\Delta \rho_g = S_f \Delta t \rho_s^{\text{mat}} \dots \dots \dots (22)$$

(iii) Isentropic phase

In this phase, we consider isentropic phenomena in a fluid governed by the following equations:

Mass equation:

$$\frac{\partial \rho}{\partial t} = -\rho (\nabla \cdot \mathbf{u}) \dots \dots \dots (23)$$

Momentum equation:

$$\frac{\partial \mathbf{u}}{\partial t} = -\frac{\nabla p}{\rho} \dots \dots \dots (24)$$

Energy equation:

$$\frac{\partial T}{\partial t} = -\frac{p_{\text{th}}}{\rho C_v} (\nabla \cdot \mathbf{u}) \dots \dots \dots (25)$$

Mass fraction of ablated vapor:

$$\frac{\partial Y_C}{\partial t} = 0 \dots \dots \dots (26)$$

VOF function:

$$\frac{\partial f}{\partial t} = 0 \dots \dots \dots (27)$$

with the EOS of $p = p(\rho, T)$.

Considering the total differential of the EOS as

$$\Delta p = \left(\frac{\partial p}{\partial \rho} \right)_T \Delta \rho + \left(\frac{\partial p}{\partial T} \right)_\rho \Delta T, \dots \dots \dots (28)$$

and Eqs. (23), (24) and (25), one can obtain the following Poisson equation for pressure:

$$-\nabla \cdot \left(\frac{\nabla p}{\rho} \right) = \frac{1}{\rho C_{sS}^2} \left[\frac{p^0 - p}{(\Delta t)^2} \right] - \frac{\nabla \cdot \mathbf{u}^0}{\Delta t} \dots \dots (29)$$

where C_{sS} is the isentropic sound velocity, p^0 and \mathbf{u}^0 are the pressure and the flow velocity after the diffusion phase. The equation presented above becomes the well known Poisson equation for pressure in the incompressible flow if ρC_{sS}^2 is much larger than the pressure variation $\frac{p^0 - p}{(\Delta t)^2}$. This equation is transformed into the wave equation for pressure in the compressive flow if the second term on the right-hand-side in Eq. (29) is negligibly small compared to the other terms. The above transition between incompressible and compressible flows is made automatically by changing the sound velocity used. The isentropic sound speed C_{sS} was derived through the EOS by the following.

$$C_{sS}^2 = \left(\frac{\partial p}{\partial \rho} \right)_S = \left(\frac{\partial p}{\partial \rho} \right)_T + \frac{p_{th}}{\rho^2} \left(\frac{\partial p}{\partial e} \right)_\rho$$

$$= C_{sT}^2 + \frac{p_{th}^2}{\rho^2 C_v T} \dots \dots \dots (30)$$

$$C_{sT}^2 = \left(\frac{\partial p}{\partial \rho} \right)_T \dots \dots \dots (31)$$

In those equations, C_{sT} is the sound velocity at constant temperature, and e is the internal energy. Quantities C_{sT} and p_{th} can be derived from the EOS.

In this isentropic phase, the Poisson equation (29) described above was first solved with the implicit method. Thereafter, the flow velocity \mathbf{u} progresses according to Eq. (24). Using updated \mathbf{u} , the mass density ρ and temperature T progress considering compressible aspects $\nabla \cdot \mathbf{u}$, according to Eqs.(23) and (25).

4. Temperature during sublimation processes

The temperature during the sublimation of materials is well known to change only slightly because of the sublimation equilibrium condition. In contrast, the temperature of the control volume in which sublimation occurs can be overestimated or underestimated during actual computation. In this work, we propose that this temperature is approximately corrected using the enthalpy-like value $\rho C_p T$ after each advection phase, diffusion phase, and isentropic phase, as shown below.

$$T^{new} = \begin{cases} \frac{\rho_g C_{pg} T^{old} + \rho_s C_{ps} T_{sub}}{\rho_g C_{pg} + \rho_s C_{ps}} & \text{(if } f > \epsilon \\ & \& T^{old} \geq T_{sub}) \\ T^{old} & \text{(otherwise)} \end{cases} \quad (32)$$

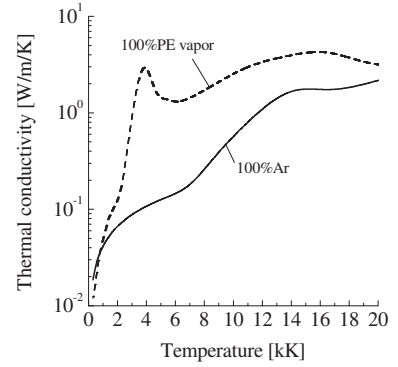


Fig.1. Thermal conductivity of 100%Ar and 100%PE vapor at atmospheric pressure as a function of temperature.

In those expressions, T_{sub} is the sublimation temperature, T^{new} is the corrected temperature, T^{old} is the temperature before correction, C_{pg} is the specific heat of gas at constant pressure, $C_{ps}(= C_{vs})$ is the specific heat of solid at constant pressure, and ϵ is a positive value to detect a control volume containing the solid.

5. Transport and thermodynamic properties

Transport properties of 100%Ar and 100% ablated vapor were calculated using the first order approximation of the Chapman-Enskog method⁽⁵⁾. Thermodynamic properties such as the mass density ρ , the specific heat at constant volume C_v , the sound velocity at constant temperature C_{sT} , and the gas constant R were calculated using the calculated equilibrium composition⁽⁵⁾. For the specific heat at constant volume C_v , for example, the following relation was used.

$$C_v = C_p + \left. \frac{\partial(RT)}{\partial T} \right|_\rho \frac{T}{\rho} \left(\frac{\partial \rho}{\partial T} \right)_p \dots \dots \dots (33)$$

$$C_p = \left(\frac{\partial h}{\partial T} \right)_p \dots \dots \dots (34)$$

$$h = \sum_j \frac{n_j}{\rho} \left(\frac{5}{2} kT + kT^2 \frac{\partial \ln Z_j}{\partial T} + \Delta H_{fj} \right) \dots \dots (35)$$

In those equations, h is the enthalpy, k is Boltzmann's constant, Z_j is the internal partition function, and ΔH_{fj} is the standard enthalpy of formation for species j .

Figure 1 presents thermal conductivity of 100%Ar and 100%PE vapor at atmospheric pressure as a function of temperature, as an example. The thermal conductivity of 100%PE vapor is much higher than that of 100%Ar at temperatures greater than 1000 K, specifically around 4000 K, because the reactional thermal conductivity by dissociation/association reactions of H_2 and C_2 contribute equivalently to the total thermal conductivity at temperatures of around 4000 K.

The transport and thermodynamic properties of mixed gas were assumed simply using the following combining rule:

$$\phi = (1 - Y_C)\phi_{Ar} + Y_C\phi_C \dots \dots \dots (36)$$

where ϕ is the combined property, ϕ_{Ar} is the property of Ar, and ϕ_{C} is the property of ablated vapor. This empirical combining rule is roughly valid for argon and additional gas mixture. It is used only for one approximation to deduce properties of mixed gas for simplicity. This rule is not always adequate for all gas combinations: it is inadequate for gas mixtures which have a large difference in ionization potential for two gases, and for gas mixtures which produce combined molecules, etc.

The properties of the control volume were deduced by combining the properties of gas and solids according to the VOF method if a control volume of interest contains gas and solids. For example, the mass density ρ in a control volume was calculated as

$$\rho = \rho_g + \rho_s, \dots \dots \dots (37)$$

where ρ_g is the mass density of gas in a control volume, ρ_s is the mass density of solid in a control volume. These values ρ_g and ρ_s are calculated with material mass density properties:

$$\rho_g = (1-f)[(1-Y_C)\rho_{Ar}^{mat}(p,T) + Y_C\rho_{C_g}^{mat}(p,T)] \dots\dots\dots (38)$$

$$\rho_s = f \rho_s^{\text{mat}}, \dots \dots \dots (39)$$

where $\rho_{\text{Ar}}^{\text{mat}}(p, T)$, and $\rho_{\text{C}}^{\text{mat}}(p, T)$ are the mass densities of Ar gas and the ablated vapor gas as a material, and ρ^{mat} is the mass density of the solid as a material.

6. Calculation condition

As described in this paper, calculation was made for a polyethylene (PE) spherical particle immersed in an Ar thermal plasma flow at atmospheric pressure as a test case. This paper describes a PE particle in Ar thermal plasmas because we have actually studied the interaction between the PE particles and Ar thermal plasmas in other experiments to study the plasma quenching effect of polymer ablated vapors⁽⁵⁾. The PE particle can be ablated easily because of its lower latent heat for ablation. Table 1 summarizes thermal properties of the solid PE particle. For simplicity, the melting process and liquid phase were neglected in this calculation. The solid PE has low thermal conductivity of about 0.34 W/m/K. Consequently, the time required for a uniform temperature distribution inside the PE particle is estimated as 0.6 s, which is much longer than the complete ablation time described later. Therefore, only the particle surface is heated strongly by the surrounding Ar plasmas. This heating causes apparent surface ablation while the solid phase is retained inside the particle, which arises from the fact that the melting process and liquid phase are rapidly passed by high heat flux from the Ar plasma under the present calculation condition. For that reason, we neglect the melting process and liquid phase. The actual melting process consumes only a little energy transferred to the particle. Therefore, the neglect of this process slightly underestimates the time necessary for complete ablation of the particle.

Figure 2 depicts a diagram of the calculation space.

Table 1. Thermodynamic properties of polyethylene.

Properties	PE
Diameter [μm]	300
Mass density [kg/m^3]	932
Evaporation temperature [K]	734
Latent heat for evaporation [kJ/kg]	75.5
Specific heat of solid [J/kg]	2408
Thermal conductivity [$\text{W}/\text{m}/\text{K}$]	0.34
Emissivity	0.3

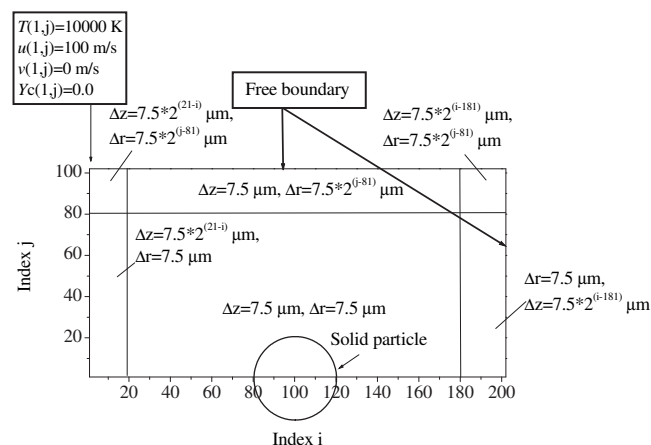


Fig. 2. Calculation space.

Two-dimensional cylindrical space (z - r coordinate) was adopted for the calculation. At the center of the calculation space, a spherical PE particle with initial diameter of $300\text{ }\mu\text{m}$ is fixed. First, we set the area of $1200\text{ }\mu\text{m} \times 600\text{ }\mu\text{m}$ on the z - r plane around the sphere particle. This area was divided into 160×80 divisions. Consequently, each of the cells in this area is a $\Delta z=7.5\text{ }\mu\text{m} \times \Delta r=7.5\text{ }\mu\text{m}$ square, where Δz and Δr respectively denote divisions for axial and radial coordinates. In this case, the particle with an initial diameter of $300\text{ }\mu\text{m}$ has 40×20 grids. Around this area, other areas were located with 20 divisions as portrayed in Fig. 2. This area was located to avoid influence from the boundary. For this purpose, the boundary was set about 4.0 m ($=4.0 \times 10^6\text{ }\mu\text{m}$) away from the particle by adopting unequal grids with increasing length using geometric progression. Adoption of boundaries far away from the particle enables a study of ablation phenomena almost in a free space. Consequently, in all, 202×102 unequal grids including cells for setting boundary values were used in this calculation.

The boundaries on the right-hand-side and the upper side were set as a free flow condition. Therefore, the gradients of all physical parameters u , v , T , p , ρ , and Y_C were set to zero at the boundaries. The Ar plasma flow comes uniformly from the left boundary of the calculation space. The gas flow velocity and the temperature of Ar plasma at the boundary on the left-hand-side of the calculation space are assumed, respectively, as 100 m/s and 10,000 K. The pressure at the inlet was fixed at 101 325 Pa atmospheric pressure. These gas flow and the temperature were adopted because the gas flow velocity of 100 m/s and the temperature of 10,000 K are

typical values in arc thermal plasmas used for thermal plasma spray coating, etc. These values are adequate for fundamental investigation of ablation phenomena in thermal plasmas.

First, we calculated the gas flow field around the particle for the initial value in the subsequent transient calculation with assumptions of the uniform temperature of 10,000 K for the calculation space including the particle inside, with no ablation of the solid particle. Using the calculated gas flow and pressure profiles around the particle as described above for the initial values, we simulated transient process including ablation around the particle in the Ar plasma flow. For this transient process, the initial temperature of the PE particle was set to 300 K. After starting the transient calculation, the surface temperature of the PE sphere particle put into the Ar thermal plasma increases because of the heat transfer from the surrounding plasma; then its surface will be ablated, thereby changing the particle surface shape. Ablated vapor produced by the particle surface ablation will change the efficiency of the heat transfer from the plasma to the particle.

7. Results

7.1 Gas flow field Figure 3(a) presents the time evolution in the flow field only near the particle. The flow velocity is denoted with flow vectors. The upper panels correspond to the time evolution in the gas flow field from $t=0 \mu\text{s}$ to $t=17.56 \mu\text{s}$; the lower panels portray those from $t=35.71 \mu\text{s}$ to $t=430.7 \mu\text{s}$. The gas flow field at $t=0 \mu\text{s}$ is the initial gas flow field that was obtained previously without consideration of ablation. At $t=0 \mu\text{s}$, the laminar gas flow is apparent around the solid sphere particle because the Reynolds number for this case is only $Re = 5.24$. With elapsed time, the particle surface temperature increases rapidly from heat transfer by the surrounding plasma; then ablation of the particle surface occurs. Ablation of the solid particle produces the gas flow jet from near the particle surface; the mass and pressure around the particle increases because of the ablation. Especially, the upstream portion of the particle surface is ablated strongly to produce gas flow, as portrayed in Fig. 3(a). That ablated gas flow goes downstream, incorporating the surrounding Ar plasma flow. In addition, the strong ablation is seen to decrease the upstream radius of the particle.

7.2 Temperature field Time evolution in the temperature distribution around and inside the particle is depicted in Fig. 3(b). Initially, the Ar plasma has a uniform temperature of 10 000 K, whereas the PE particle has a uniform temperature of 300 K at $t=0 \mu\text{s}$. At $t=1.371 \mu\text{s}$, the plasma temperature around the particle decreases rapidly, chiefly by thermal conduction. Thereafter, such a reduced temperature area spreads downstream because the ablated vapor near the evaporation temperature is transported mainly by convection.

7.3 Mass fraction of ablated vapor Figure 3(c) presents the time evolution in the mass fraction of ablated vapor to Ar. At $t=0 \mu\text{s}$, no ablated vapor exists in the calculation space. After starting calculation, ab-

lation occurs rapidly to produce ablated vapor around the particle. At $t=1.371 \mu\text{s}$, results show that the region with an ablated vapor mass fraction of 10^{-3} reaches $225 \mu\text{m}$ upstream away from the upstream particle surface. This is one cloud of ablated vapor. This transport of the ablated vapor around the particle at this time was mostly attributed to its diffusion. Subsequently, the ablated vapor ejected from the particle surface is transported by a combination of diffusion and convection to the downstream region. After $t=8.736 \mu\text{s}$, the region with an ablated vapor mass fraction of 10^{-3} , which is an ablated vapor cloud, reaches $300 \mu\text{m}$ upstream away from the upstream surface of the particle. The region's thickness remains mostly unchanged during ablation.

7.4 Change in the particle shape In this work, the surface change of the particle is tracked using the VOF function f . Figure 4 presents the VOF function profile at $t=0 \mu\text{s}$, $t=183.0 \mu\text{s}$, $t=430.7 \mu\text{s}$, $t=1358 \mu\text{s}$, and $t=1794 \mu\text{s}$. The VOF function outline corresponds to the particle surface. As shown there, the particle shape changes by ablation. From $t=0 \mu\text{s}$ to $t=183.0 \mu\text{s}$, the left half surface of the particle is ablated almost uniformly. From $t=183.0 \mu\text{s}$ to $t=1794 \mu\text{s}$, the upstream surface perpendicular to the flow on the axis is ablated more strongly, resulting in the reduction of the axial 'radius' of the particle. Thereafter, the particle volume is reduced rapidly. This result is considered reasonable because high heat flux from the plasma comes from the upstream plasma flow; the ablated vapor is transported quickly downstream, as portrayed in Fig. 3.

8. Discussion

8.1 Comparison to calculation results without ablation Calculation was conducted for comparison without consideration of ablation phenomena. Figures 5(a) and 5(b) indicate the gas flow and temperature fields around the particle, respectively, without consideration of ablation phenomena. If ablation does not occur, the gas flow field only slightly changes from the initial gas flow field with time. The temperature around the particle decreases with time, mainly because of thermal conduction. A comparison of Fig. 3 to Fig. 5 reveals clearly that ablation produces strong gas flow near the particle surface, and that the produced strong gas flow transports low-temperature ablated vapor from the surface to the downstream region of the particle. This low-temperature transport decreases the temperature near the particle and downstream of it.

8.2 Rough estimation of the complete ablation time The complete ablation time is often estimated using the following simple energy equation.

$$4\pi r_{\text{pol}}^2 \rho_{\text{pol}} L \frac{\partial r_{\text{pol}}}{\partial t} = h_{\text{trans}} (T_{\infty} - T_{\text{wall}}) \pi r_{\text{pol}}^2 \cdot (40)$$

Therein, r_{pol} is the radius of the particle, ρ_{pol} is the mass density of the solid polymer, h_{trans} is the heat transfer coefficient for a sphere in a convection flow, T_{∞} is the temperature of Ar plasma far away from the particle, and T_{wall} is the temperature of the particle surface. This equation assumes the uniform temperature distribution

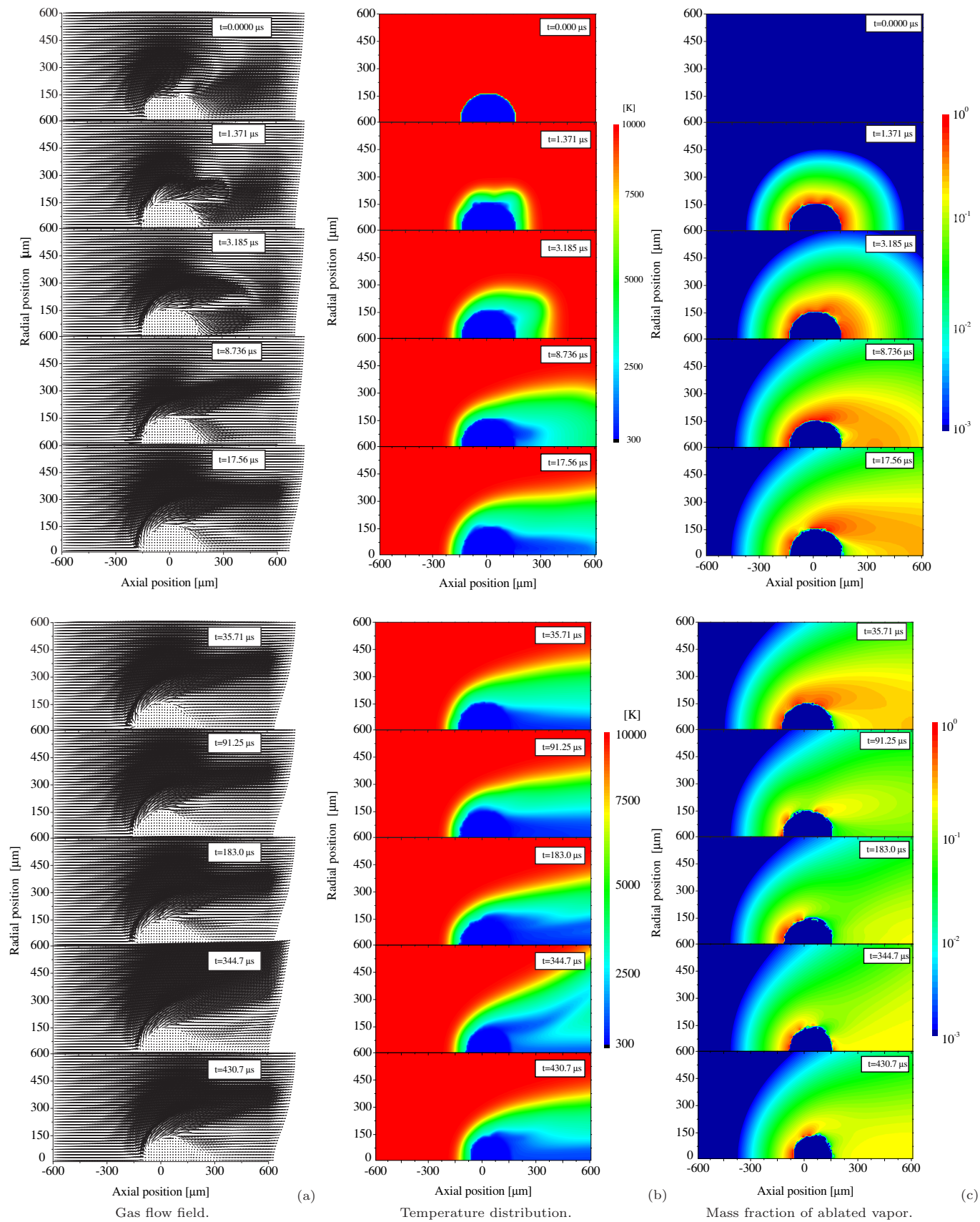


Fig. 3. Gas flow, temperature and ablated vapor distributions around the PE particle in Ar plasma flow.

inside the particle and the uniform heat flux irradiated on the whole surface of the particle. From this equation,

the complete ablation time was estimated roughly as $360 \mu\text{s}$. This value is about one-sixth shorter than the result

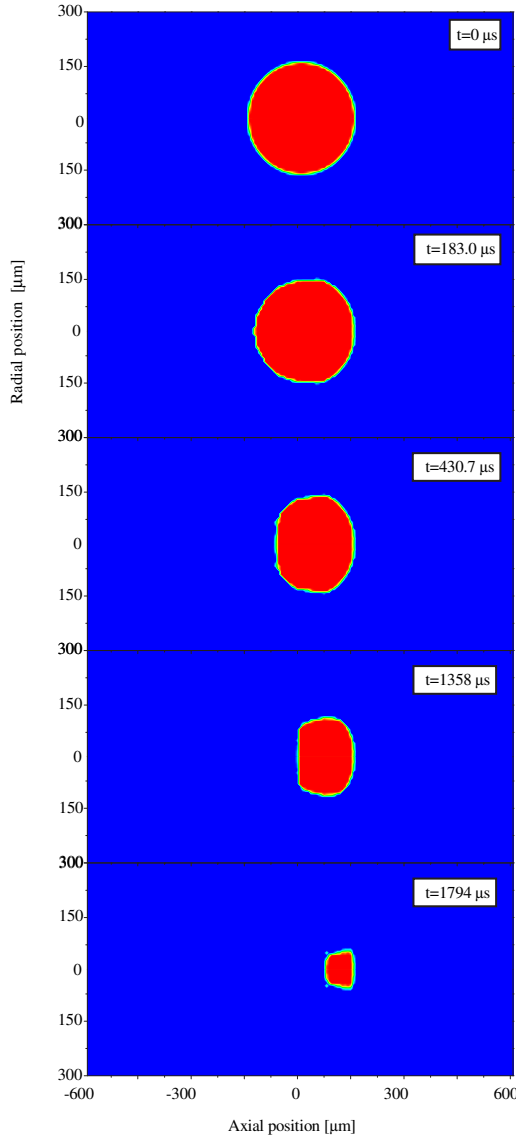
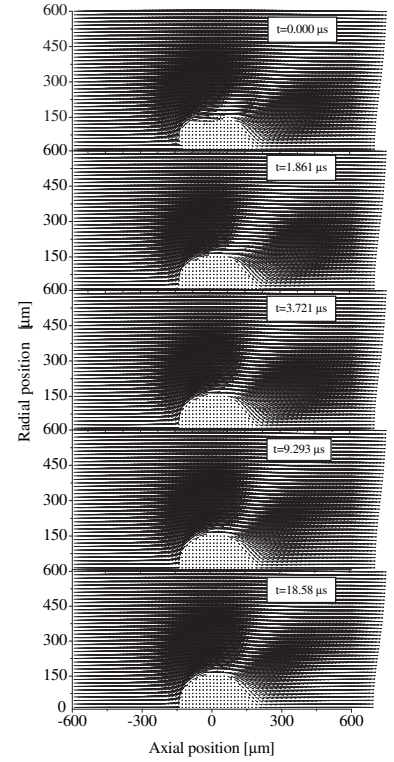


Fig. 4. VOF function.

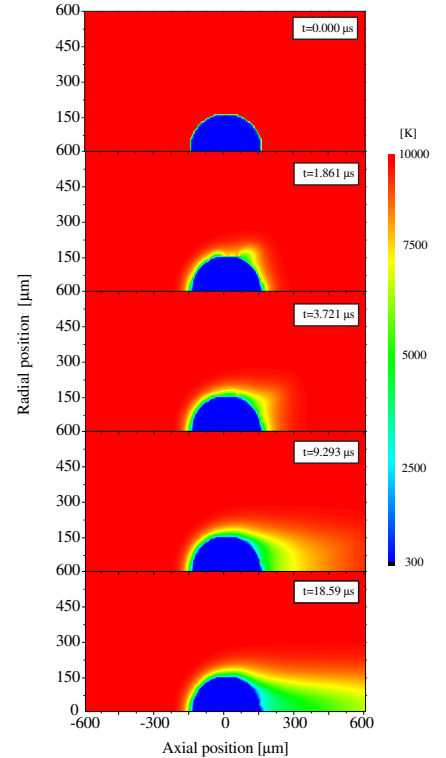
from the calculation present in this paper. The shorter ablation time might be attributed to the fact that no shielding effect exists from the ablated vapor in case of this rough estimation of complete ablation time. In other words, ablation produces an ablated vapor cloud around the particle, which shields it from the heat of the surrounding hot plasma.

9. Conclusion

Modelling was performed for ablation of a solid particle in a thermal plasma considering interactions between the solid particle and the thermal plasma. The model was developed based on the CIP-CUP method. The VOF function was adopted to track the boundary of the solid particle. Using the developed model, the ablation process of a polyethylene spherical particle in a thermal plasma was simulated. This model can predict the phase transition and shape change of a solid particle. Strong ablation is apparent at the upstream surface of the particle. The model also enables prediction of the ablated vapor cloud thickness around the particle as



(a) Gas flow field.



(b) Temperature field.

Fig. 5. Gas flow and temperature fields without consideration of ablation of a PE particle in Ar plasma.

300 μm . The developed model can predict ablation phenomena in thermal plasmas such as interaction between electrodes and arc plasmas, and polymer ablation in a

circuit breaker.

References

- (1) T. Yamada, and T. Abe: "Plasma and the Flight Environment of the HAYABUSA Reentry Capsule", *J. Plasma Fusion Res.*, **82**, 368–374 (2006).
- (2) T. Yabe, T. Ishikawa, P.Y. Wang, T. Aoki, Y. Kadota and F. Ikeda: "A Universal Solver for Hyperbolic Equations by Cubic-Polynomial Interpolation II. Two- and Three- Dimensional Solvers", *Comput. Phys. Commun.* **66**, 233–242 (1991).
- (3) T. Yabe, F. Xiao and T. Utsumi: "Constrained Interpolation Profile Method for Multiphase Analysis", *J. Comput. Phys.*, **169**, 556–593 (2001).
- (4) J. Mostaghimi, M. Pasandideh-Fard, S. Chandra, "Dynamics of Splat Formation in Plasma Spray Coating Process", *Plasma Chem. & Plasma Process.*, **22**, 59–84 (2002).
- (5) Y. Tanaka, Y. Takeuchi, T. Sakuyama, Y. Uesugi, S. Kaneko and S. Okabe: "Numerical and Experimental Investigations on Thermal Interaction between Thermal Plasma and Solid Polymer Powders using Induction Thermal Plasma Technique", *J. Phys. D: Appl. Phys.*, **41**, 025203 (2008).

Yasunori Tanaka (Member) received B.S., M.S., and Ph.D.



degrees in electrical engineering from Nagoya University, Japan, in 1993, 1995 and 1998, respectively. In April 1998, he was appointed a Research Associate at Kanazawa University, Japan. He has been working as an Associate Professor at that university since August 2002. One of his papers was selected as a leading paper in Journal of Physics D: Applied Physics in 2004. His research interests include funda-

mentals and applications of thermal plasmas and arc interruption phenomena. He is a member of IEE of Japan, and is a member of Plasma and Fusion Research.

Javad Mostaghimi (Non-member) received a B.Sc. de-



gree from Sharif University, Iran, in 1974, and M.Sc. and Ph.D. degrees in Mechanical Engineering from the University of Minnesota, Minneapolis, in 1978 and 1982, respectively. He held positions at Pratt & Whitney Canada, Longueuil, Quebec, and at the Department of Chemical Engineering, University of Sherbrooke, Sherbrooke, Quebec. In 1990, he joined the Department of Mechanical and Industrial Engineering, University of Toronto, Ontario, where he is

currently a Professor. His main research interests are the study of thermal spray coatings, transport phenomena, and electromagnetics in thermal plasma sources.

He is a Fellow of the International Union of Pure and Applied Chemistry (IUPAC) and the American Society of Mechanical Engineering (ASME). He is also a member of the editorial board of Plasma Chemistry and Plasma Processing.